ACS APPLIED BIO MATERIALS

www.acsabm.org Article

Fabrication of Conductive, Adhesive, and Stretchable Agarose-Based Hydrogels for a Wearable Biosensor

Qingquan Han, Anhe Wang,* Wei Song, Milin Zhang, Shengtao Wang, Peng Ren, Linna Hao, Jian Yin,* and Shuo Bai*

Cite This: https://doi.org/10.1021/acsabm.1c00501 Read Online

ACCESS | Metrics & More | Article Recommendations | Supporting Information

ABSTRACT: Herein, a strategy is proposed to prepare a conductive, self-adhesive, and stretchable agarose gel with the merits of distinct heat resistance, freeze resistance, and long-term moisture retention. To endow the gels with conductivity, monodisperse carbon nanotubes modified by polydopamine are introduced into the gel networks, which promote both conductivity and mechanical strength of the gels. Meanwhile, further addition of glycerol enhances excellent stretchability as well as heating/freezing tolerability and moisture retention of the gels. A wearable biosensor based on the gel is fabricated to record body motions precisely with good biocompatibility, which benefits the development of smart wearable devices.

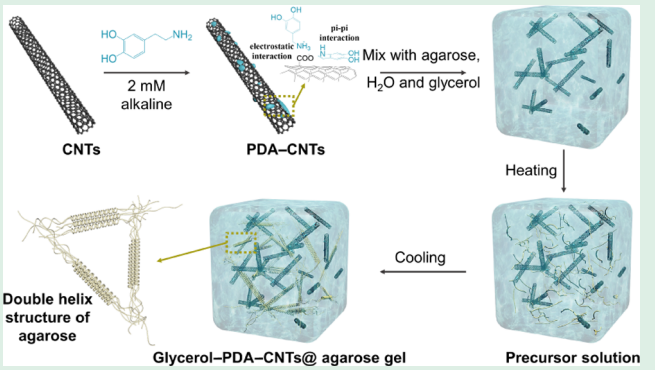

KEYWORDS: *agarose hydrogel, conductive, adhesive, stretchable, moisture retention*

1. INTRODUCTION

The smart wearable devices have gained tremendous attention due to their great potential applications in personal health monitoring, trauma treatment, and prognosis.[1−7] Various materials such as metallic yarn, polyethylene terephthalate, silica gel, and glass fabric have been applied to construct wearable devices with distinct functions. However, they more or less suffer from mismatched mechanical properties with body tissue, poor biocompatibility, less stretchability, and adhesiveness.[8−11] To solve the above issues, hydrogels composed of water and polymer fibers have been developed due to their similarities to body tissue and have become a promising material candidate for next-generation wearable devices.[12−15] So far, some wearable devices based on hydrogels have been constructed, including polyacrylic acid, polyacrylamide, polydimethylsiloxane, and polyurethane.[16−19] However, these polymer hydrogels are hard to avoid the risk of causing allergies and irritation to the human body because of toxic monomers or byproducts during synthetic procedures and decomposition processes, preventing their further applications.[20−23]

Agarose, as a natural polysaccharide and good candidate, has been widely studied owing to its wide variety of sources, biocompatibility, biodegradability, and hypoallergenicity. Meanwhile, agarose hydrogels can be easily prepared through heating and cooling processes.[24] Until now, some wearable devices based on agarose hydrogels have been reported.[25,26] However, most agarose hydrogels show insufficient mechanical strength to bear the damage caused by external deformation during application in wearable devices. Incorporation of biocompatible nanoparticles is a facile route to enhance the strength.[27−29] Among these particles, the carbon nanotube (CNT) with good conductivity and nontoxic properties is a promising material to enhance the tensile strength and conductivity of hydrogels.[30,31] Unfortunately, incorporation of CNTs usually results in decreased stretchability because of the inhomogeneous distribution of hydrophobic CNTs, causing microdefects and decreasing the mobility of the polymer chain within the hydrogel.[32] To solve the problem, surface modification attracts considerable interest for functionalizing substrates and enhancing the hydrophilicity and biocompatibility of substrates.[33−35] Nevertheless, this process is complicated particularly and not easy to control the polymerization process, leading to particle aggregation and unnecessary agent waste.

Excellent tissue adhesion is also a crucial factor for wearable devices, which determines the normal operation of devices and their signal-to-noise ratio. At present, various materials have been developed to enhance the self-adhesion strength of

Received: April 30, 2021
Accepted: June 15, 2021

Scheme 1. Schematic Illustration of the Preparation of PDA−CNTs@Agarose Gels

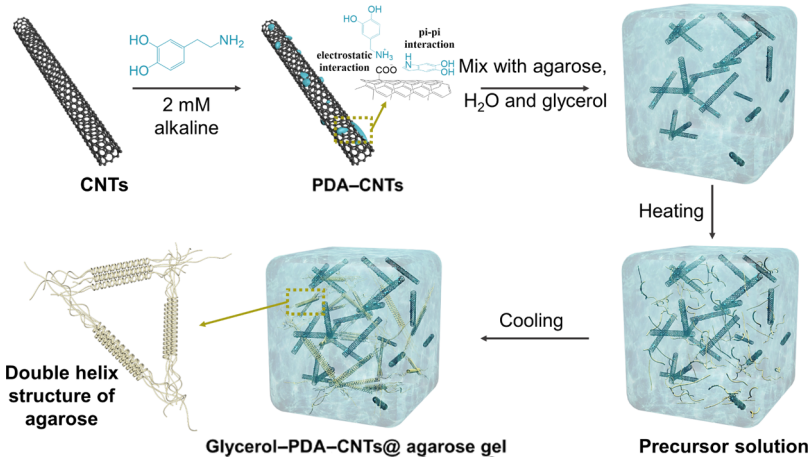

hydrogels.[36−41] Especially glycerol, as a mild and cheap accessory ingredient, has been applied in adhesives,[42,43] and some works have verified that the free hydroxyl groups of glycerol may contribute to the adhesive property of materials.[44] Furthermore, the introduction of glycerol into hydrogels can improve the anti-heating, anti-freezing, and moisture retention capabilities of the gel, displaying a great potential application in the construction of wearable devices.

In this work, we report a facile approach to fabricate a wearable motion sensor based on a biocompatible, conductive, stretchable, and self-adhesive agarose gel (Scheme 1). First, CNTs are modified by polydopamine (PDA) to improve their distribution in agarose hydrogels, which not only promotes the conductivity of the gel but also enhances the mechanical strength. During the polymerization process, dopamine (DA) concentrations are adjusted to avoid the aggregation of PDA and unnecessary agent waste. Furthermore, the introduction of glycerol makes the gels possess a significant improvement in tissue adhesion strength (1.2 kPa), stretchability (more than 120% elongation), and heating (60 °C) and freezing (−20 °C) resistance. Experimental data demonstrate that the wearable motion sensor based on the gels is capable of detecting body motions, indicating the promising application in wearable devices.

2. MATERIALS AND METHODS

2.1. Materials. Agarose (low gelling temperature) and DA hydrochloride were purchased from Sigma-Aldrich (USA). CNTs (single-walled, hydroxylation) were purchased from Shanghai Aladdin Biochemical Technology Co., Ltd. Glycerol was purchased from Beijing Chemical Works. All chemicals used here were of reagent grade without further purification. The water used in all experiments was purified with a Milli-Q integral A 10 system from Millipore Co., Ltd.

2.2. Synthesis of Polydopamine−Carbon Nanotubes. PDA−CNTs were synthesized via an alkali-induced oxidation and self-polymerization method. Briefly, DA and CNT powders were added to Tris-HCl buffer (pH = 8.5, 10 mM) under stirring for 12 h, which made DA self-polymerized in the atmosphere. Then, PDA−CNTs were obtained through three cycles of centrifugation and washing with deionized water. Finally, PDA−CNTs were resuspended in deionized water with different concentrations and stored at 4 °C for further use. Contents of DA−CNT reaction mixtures are listed in Table S1.

2.3. Preparation of Glycerol−PDA−CNTs@Agarose Gels. The gels were obtained through the sol−gel transition of agarose solution induced by temperature change. Briefly, agarose powder and PDA−CNT suspension were mixed together in deionized water, and then, glycerol was added to the above mixture. A homogeneous suspension was obtained under stirring, which was heated at 90 °C until agarose dissolved completely. Finally, the hot agarose solution was poured into a suitable mold, and gels were formed after cooling to room temperature. Typical compositions of the gels are listed in Table S2.

2.4. Cytotoxicity Test. To evaluate the cytotoxicity of glycerol−PDA−CNTs@agarose (G−P−C@agarose) gels, NIH3T3 cells were used as a cell model. Phosphate-buffered saline (PBS) and pure agarose gels were set to a negative and positive control, respectively. The CCK-8 assay was used to quantify the relative cell viability after 1 and 2 days of coculturing. The cell morphology was observed by confocal laser scanning microscopy (CLSM, SP8 STED 3X, Leica, Germany) after stained by calcein-AM/PI. The experimental details are available in the Materials and Methods section of the Supporting Information.

2.5. Dermal Irritability Test. Mouse (BALB/c) skin irritation experiments were carried out to assay the dermal irritability of the gels. At first, an electric razor was used to clip the hair of mice's backside, and depilatory paste (Veet, Reckitt Benckiser, China) was used for the further removal of villi. After that, all mice were randomly divided into three groups including PBS-, commercial ECG gel-, and G−P−C@agarose gel-treated groups. The gel samples were cut into a small cylinder with a 15 mm diameter and 2 mm thickness, and PBS was equal in quality to gels. Subsequently, gels and PBS were pasted and spread over the depilated skin (15 mm diameter), respectively. The areas were covered by medical nonwoven fabric and observed after 24 h.

2.6. Motion Detection by the G−P−C@Agarose Gel Sensor. The G−P−C@agarose gel sensor was designed as rectangular piece-like with a 20 mm length, 10 mm width, and 2 mm thickness. The gel was connected to the leads, and the real-time variation of electrical signals was recorded by a CHI 660E equipment. The amperometric $i-t$ curve method was applied, and the initial E was set at 0.8 V. We pasted the gel sensor on the finger joint, inner wrist, elbow joint, and back to collect real-time signals during the bending process. It is worth noting that the relative changes of resistance were calculated by Ohm's law.

3. RESULTS AND DISCUSSION

3.1. Synthesis Strategy of the G−P−C@Agarose Gel. The G−P−C@agarose gel was fabricated with a two-step's method. As shown in Scheme 1, the first step involved the synthesis of PDA−CNTs through modifying CNTs with PDA. The second step related to the mixture of PDA−CNTs and agarose with deionized water and glycerol to obtain a homogeneous precursor solution, which was heated above 90

https://doi.org/10.1021/acsabm.1c00501
ACS Appl. Bio Mater. XXXX, XXX, XXX−XXX

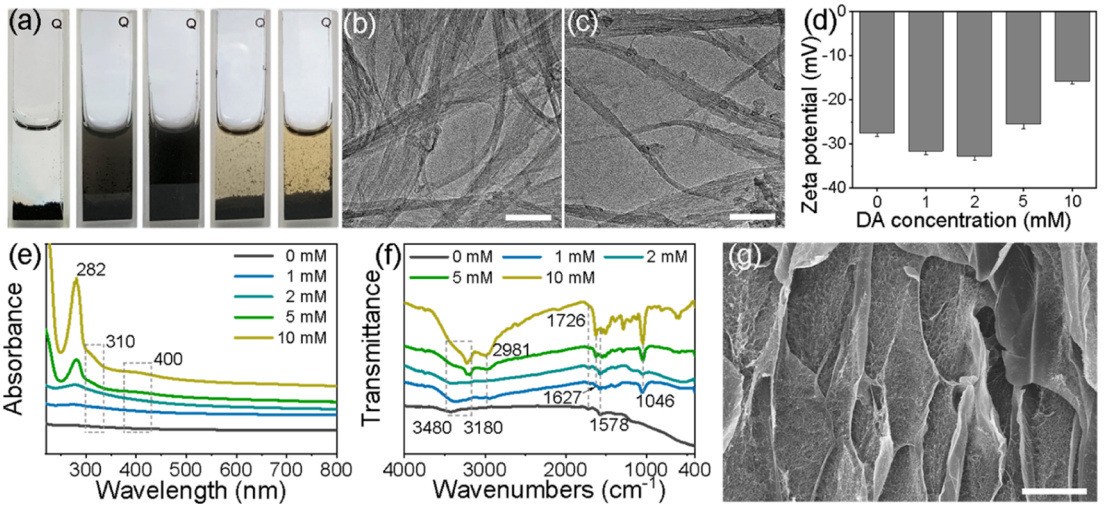

Figure 1. (a) Photographs of PDA−CNT solutions with different concentrations of DA (0, 1, 2, 5, and 10 mM from left to right, respectively). (b) TEM image of raw CNTs and (c) PDA−CNTs; scale bar = 100 nm. (d) Zeta potential of PDA−CNTs with different concentrations of DA. (e) UV−vis and (f) FTIR spectrum of PDA−CNTs with different concentrations of DA. (g) SEM image of the PDA−CNTs@agarose hydrogel; scale bar = 20 μm.

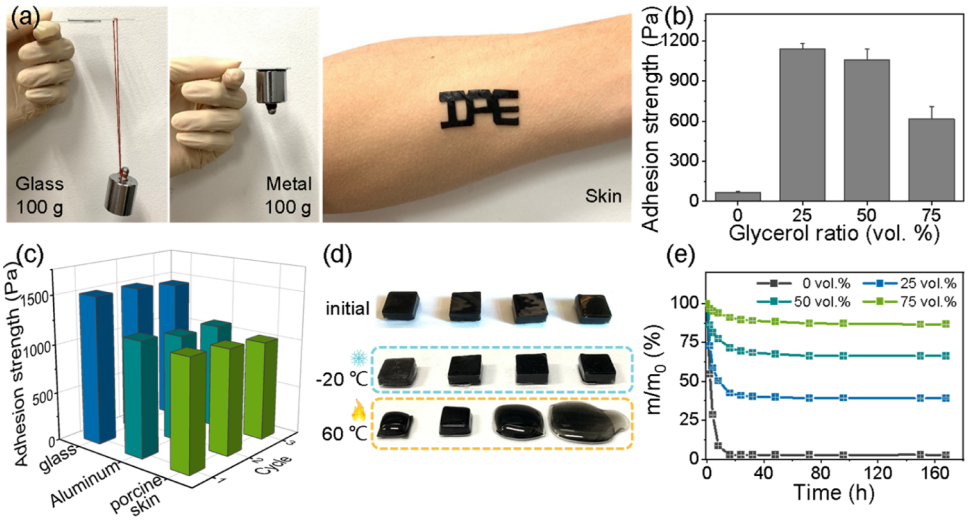

Figure 2. (a) Adhesiveness of G−P−C@agarose gels to glass, metal, and skin. (b) Average adhesion strength of the gels with different glycerol contents to porcine skin. (c) Repeatable adhesion of the gels to different substrates (glycerol contents, 25%, vol %). (d) Photographs of the gels with different contents of glycerol after incubation in −20 or 60 °C for 6 h. (e) Variation of the residual mass of the gels with different contents of glycerol during exposure to the air atmosphere for 168 h.

°C to make the PDA−CNTs and glycerol distribute well in agarose gels after cooling.

3.2. Characterization of Polydopamine−Carbon Nanotubes. DA was used to modify the surface of CNTs through oxidative polymerization under alkaline conditions (pH = 8.5), which could improve the hydrophilicity of CNTs in aqueous solution. It is known that DA polymerization was influenced by various factors including concentration, pH value, oxidant, temperature, and pressure.[45] Herein, the effect of DA concentration on the dispersity of CNTs was investigated in detail. From the photographs in Figure 1a, CNTs obviously illustrated improved dispersity in aqueous solution when modified by PDA. When the concentration was increased to 2 mM, CNTs possessed the best dispersity in aqueous solution. Further increasing the concentration would lead to the aggregation of CNTs, which could be ascribed to the larger size of PDA nanoparticles formed outside CNTs due to too high monomer concentration.[46,47] Furthermore, the morphology change of CNTs before and after PDA modification was assayed by transmission electron microscopy (TEM), as shown in Figure 1b,c. It is obvious that raw CNTs were smooth, while PDA−CNTs illustrated some particles on their surface. In addition, the energy-dispersive spectroscopy (EDS) mapping of PDA−CNTs revealed the presence of nitrogen atoms which could be assigned to PDA (Figure S1), demonstrating the successful PDA modification.

To evaluate the dispersity of CNTs in aqueous solution after PDA modification, dynamic light scattering and zeta potential experiments were performed. From the data in Figure 1d, the zeta potential of CNTs gradually decreased along with increasing DA concentration from 0 to 2 mM and then increased as the concentration was higher than 2 mM. It is reported that the dispersity and stability of objects in aqueous solution could be affected by surface charge strongly.[48] Objects

https://doi.org/10.1021/acsabm.1c00501
ACS Appl. Bio Mater. XXXX, XXX, XXX−XXX

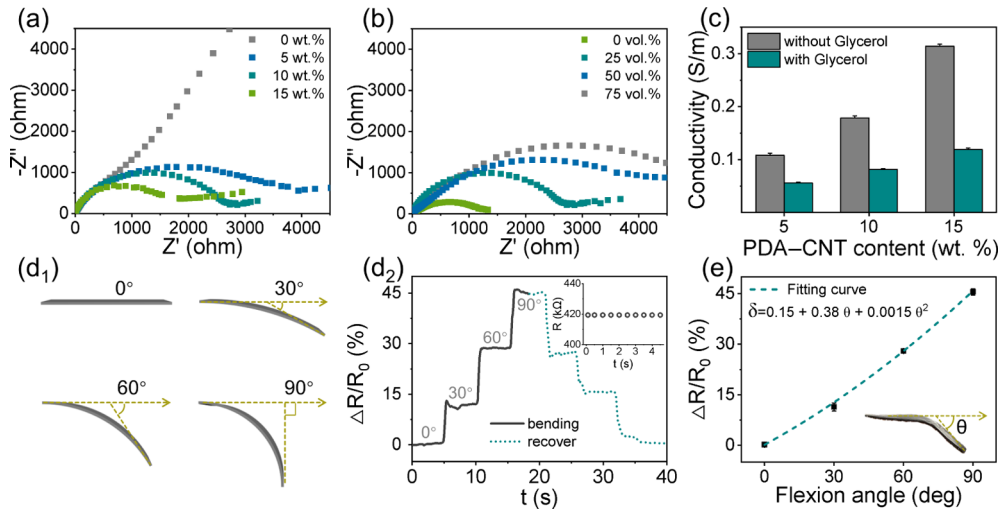

Figure 3. AC impedance curves of various gels with (a) different contents of PDA−CNTs and (b) glycerol, respectively. (c) Conductivity of gels with and without glycerol. (d_1) Models of gels in different bending status and (d_2) the corresponding real-time relative resistance changing during the bending−recovery process. Inset: resistance fluctuation during the test. (e) Relative resistances as a function of the bending angle from 0 to 90°. Inset: definition of the flexion angle at θ angle.

possessed better dispersity as their zeta potential stayed away from neutrality. Herein, when the DA concentration was 2 mM, the minimum zeta potential of PDA−CNTs was −32.8 ± 0.8 mV, which was thought to have the best dispersity, similar to the result in Figure S2. Therefore, CNTs modified by 2 mM DA were applied in the following experiment, unless otherwise noted.

In addition, Fourier-transform infrared spectrometry (FTIR) and UV−vis analysis were performed to further assay the formation of PDA on the surface of CNTs. As shown in Figure 1e, peaks at 282, 310, and 400 nm could be assigned to the characteristic absorption of catechol groups, $\pi-\pi^*$ transition of C═C/C═N, and the color change of solution, respectively.[49−51] FTIR spectra also provided the same results, as displayed in Figure 1f. A peak at 1726 cm^{-1} could be ascribed to the stretching vibration of C═O, indicating the oxidation of hydroxyl groups. Additionally, a peak at 1627 cm^{-1} was attributed to the aromatic C═C stretching vibration of indole, which was a typical absorption of PDA, and peaks at 1578 and 1046 cm^{-1} were assigned to aromatic C═C/pyrrole ring stretching and CH in-plane/CH out-of-plane bending vibration, respectively,[52−54] demonstrating the successful PDA modification.

The scanning electron microscopy (SEM) cross-sectional image of the freeze-dried hydrogel displayed PDA−CNTs randomly interweaved within the agarose fibrous network (Figure 1g). It indicated that CNTs could be distributed evenly throughout the gel network after modification, which benefited electron transportation and hydrogel reinforcement. It is worth noting that the oxidative polymerization of DA was inhibited by glycerol (Figure S3). Therefore, it is not suitable to prepare the G−P−C@agarose gel via a one-pot method.

3.3. Self-Adhesive, Anti-Heating, Anti-Freezing, and Moisture Retention Properties. Glycerol had been applied in adhesives widely due to its excellent biocompatibility and safety. To endow the agarose gel with adhesiveness, glycerol was introduced into the gels. Interestingly, the prepared G−P−C@agarose gels exhibited excellent self-adhesive properties to various substrates, including glass and metals (Figure 2a), which could bear 100 g weight without obvious break and cracks. The quantitative data depictured in Figure S4a showed that adhesion strengths of gels to glass and aluminum were about 1510 and 1170 Pa, respectively (glycerol contents, 25%, vol %).

In addition, G−P−C@agarose gels could tightly adhere to the skin of the forearm and remained intact after strenuous exercise of the forearm, suggesting that the G−P−C@agarose gels had great potential applications in wound dressings and tissue engineering. To further quantify the adhesion strength of the gel to tissue, a shear adhesion test was conducted. Herein, porcine skin was employed as substrates to mimic the human skin tissue. As shown in Figure 2b, G−P−C@agarose gels without glycerol showed a weak adhesion with a value of about 67 ± 8 Pa, which attributes to the property of PDA. The adhesion strength illustrated sharp improvement as the glycerol content ranges from 0 to 25 vol %, displaying the best adhesion strength to porcine skin with a value of about 1140 ± 40 Pa. In contrast, the strength gradually decreased as the glycerol content was beyond 25%, which could be ascribed to the spilling of glycerol causing relative slip of the gel and porcine skin. The displacement−shear adhesion strength curves are displayed in Figure S4b.

The reusability of G−P−C@agarose gels was crucial for their application of wearable devices. The reusable adhesion ability of the G−P−C@agarose gel was evaluated by repeating to stick and peel off the gels to different substrates. As shown in Figure 2c, G−P−C@agarose gels illustrated excellent reusability. No obvious loss in adhesion strength could be observed for three cycles, which achieved to be about 1450, 1090, and 1020 Pa to glass, aluminum, and porcine skin, respectively.

Incorporation of glycerol not only endowed gels with self-adhesion ability but also enhanced the anti-heating, anti-freezing, and moisture retention properties. First, the anti-heating and -freezing properties of G−P−C@agarose gels with different glycerol contents were tested at 60 and −20 °C, respectively. As depictured in Figure 2d, gels without glycerol were frozen at −20 °C. However, gels with various contents of glycerol could keep their initial hydrogel state due to the inhibitory effect of glycerol on ice crystallization.[55] During the

https://doi.org/10.1021/acsabm.1c00501
ACS Appl. Bio Mater. XXXX, XXX, XXX−XXX

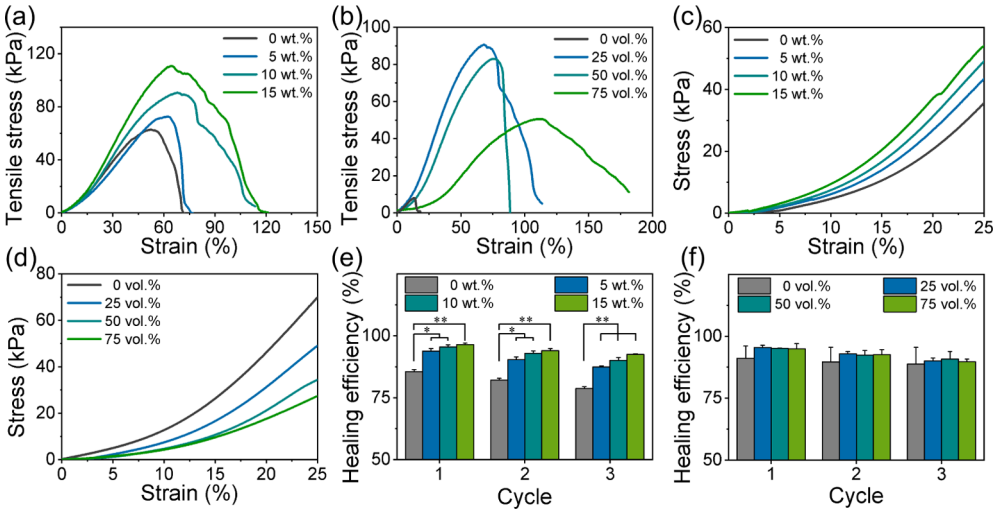

Figure 4. Tensile stress−strain curves of the gels with different contents of (a) PDA−CNTs and (b) glycerol. Compress stress−strain curves of the gels with different contents of (c) PDA−CNTs and (d) glycerol. Healing efficiency comparison of the gels with different contents of (e) PDA−CNTs and (f) glycerol.

anti-heating experiment, gels without glycerol showed obvious shrink after heating at 60 °C for 6 h. In contrast, the presence of glycerol prevented excessive dehydration of gels and kept the initial gel state. However, the gels would deform slightly after heating as the glycerol content increases above 50% (vol %).

Furthermore, the moisture retention property of gels was assayed by monitoring water loss from gels. As shown in Figures 2e and S5, gels without glycerol lost moisture quickly in 24 h, while gels with glycerol could hold water up to 39.2 ± 0.5, 66.3 ± 0.4, and 86.6 ± 0.2% in 168 h as the content of glycerol was 25, 50, and 75% (vol %), respectively. It may be because glycerol lowered the vapor pressure of water through hydrogen bond interaction with water molecules.[56]

3.4. Conductivity of G−P−C@Agarose Gels. Single-wall CNTs possessed excellent conductivity and could distribute in agarose gels well after PDA modification, which significantly enhanced the conductivity of agarose gels (Figure S6). To quantitatively determine the influence of PDA−CNTs and glycerol contents on conductivity, agarose gels with different contents of PDA−CNTs and glycerol were tested by an electrochemical workstation. As displayed in Figure 3a, AC impedance curves revealed that the conductivity of gels was dependent on the doping amount of PDA−CNTs. It could be explained by the fact that an increased amount of CNTs provided more paths for electron transportation.[57] In contrast, elevating the glycerol content could reduce the conductivity of gels (Figure 3b), decreasing from maximum 0.32 to 0.12 S/m (Figures 3c and S7). It is attributed to the nonelectrolyte property of glycerol.[58] Therefore, it is necessary to optimize the glycerol contents meeting the requirements of both conductivity and self-adhesive strength.

The consistent variation in electronic signals induced by external deformation was an important factor for the application of conductive gels. To test this property, various bending models of G−P−C@agarose gels were constructed and illustrated, in which the flat status of gels was defined as 0° of bending (Figure 3d$_1$). The relative resistances of gels under bending at 0, 30, 60, and 90° were calculated by Ohm's law through real-time potential and current values. From the data in Figure 3d$_2$, G−P−C@agarose gels displayed a clear step-like trend, demonstrating that the gels possessed good accuracy and reversibility properties in resistance changing. Besides, the inset graph showed that the resistance of gels kept constant under a certain bending status, indicating that the gels could generate continuous and stable electrical signals. Furthermore, the relationship between the relative resistance variation and flexion angle of the gel was curve-fitted (Figure 3e). The relative resistance change (δ) could be calculated by the following equation during 0−90°, $\delta = 0.15 + 0.38\theta + 0.0015\theta^2$, where θ is the bending angle of the gels.

In addition, the conductive self-healing efficiency of G−P−C@agarose gels was verified by the cutting−healing test for six cycles. As shown in Figure S8a, the gel was connected in series with a light emitting diode (LED) bulb in the circuit. After switching on the LED bulb, the gel was cut into two pieces and the bulb went out immediately. However, the bulb lighted again once the two divided gels contacted together, indicating the excellent conductive self-healing efficiency of gels. To further investigate the self-healing process, the gels underwent a process of cutting and subsequent contacting together with six cycles; the real-time variation of resistance in Figure S8b showed no obvious change. Furthermore, the conductive healing efficiency could achieve up to 93% after six cutting−healing cycles (Figure S8c), indicating that the gels possessed excellent electrical healing capability.

3.5. Mechanical Properties of G−P−C@Agarose Gels. As reported in previous works, the introduction of CNTs and glycerol could improve the mechanical strength and shear recovery capability of the gels.[59−63] Figure 4a illustrates that the tensile strength of gels was strongly enhanced from 62 to 111 kPa as the content of PDA−CNTs increased from 0 to 15% (wt %), while the ruptured elongation of gels was improved in the range of 54−67%. Moreover, the further addition of glycerol significantly increased the ruptured elongation of 66, 78, and 115%, as well as the tensile strength of 90, 83, and 51 kPa (Figure 4b) when the content of glycerol was 25, 50, and 75% (vol %), respectively. It could be explained by the fact that the presence of glycerol improved the mobility of agarose chains under external force, resulting in a soft and flexible nature enough to bear deformation. Similar results were obtained from the uniaxial compress test (25%

https://doi.org/10.1021/acsabm.1c00501
ACS Appl. Bio Mater. XXXX, XXX, XXX−XXX

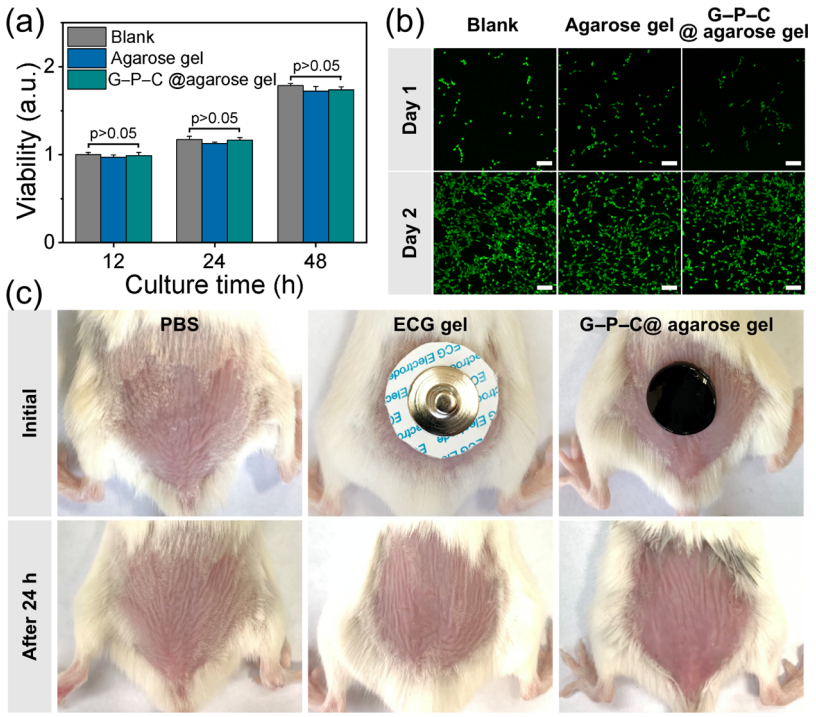

Figure 5. (a) CCK-8 assay of NIH3T3 cells after coculturing with and without gels for 1 and 2 days. (b) Confocal images of NIH3T3 cells, and the cells were stained with calcein-AM/PI; scale bar = 100 μm. (c) Dermal irritation test of PBS, commercial ECG gel, and G−P−C@agarose gels.

strain); the compression strength increased from 35 to 54 kPa along with the increasing addition of PDA−CNTs but decreased from 70 to 27 kPa as the content of glycerol increased (Figure 4c,d).

Rheological behaviors of gels were also investigated to determine the healing efficiency under shear stress. As shown in Figure S9, G' (storage modulus) was higher than G'' (loss modulus) at the beginning, indicating that the gel was kept intact. Then, both G' and G'' sharply decreased and G' was lower than G'' when a high amplitude oscillatory (100%, 1 Hz) was applied, implying that the gel was destroyed and converted into a fluid state. Subsequently, G' exceeded G'' immediately after the declining of amplitude oscillatory, which suggested the self-healing of the gels. After three cycles, the G' values of the gels were used to analyze the healing efficiency of gels.[64,65] From the data displayed in Figure 4e, the incorporation of PDA−CNTs promoted the self-healing of gels significantly by enhancing the mechanical strength. The higher the content of CNTs the gels had, the higher the healing efficiency the gels achieved. Moreover, the presence of glycerol may not significantly affect the recovery performance of the gels (Figure 4f).

3.6. Safety of the G−P−C@Agarose Gel. Material safety was crucial for their applications in wearable devices. First, the biocompatibility of G−P−C@agarose gels was assayed by taking the NIH3T3 cell as a model. The CCK-8 data in Figure 5a illustrated that the viability of cells coincubated with the G−P−C@agarose gel had no obvious change compared with that of the control group after 2-day culturing, indicating their good affinity to NIH3T3 cells. In addition, the morphologies of cells were observed by CLSM after calcein-AM/PI staining. As shown in Figure 5b, almost no dead cells were observed over CLSM images and the cells maintained their activity of proliferation after 2-day incubation with gels, similar to the results of the CCK-8 experiment.

Nonirritant was another important factor for body-used materials. A dermal irritability test was performed to assess the irritation of G−P−C@agarose gels to skin tissues.[66] A mouse (BALB/c) model was used to mimic the human skin tissue. PBS and a medical ECG electrode were chosen as the negative and positive control, respectively. The gel sample was cut into smaller pieces with a 15 mm diameter, and the observation was carried out after pasting the piece to the backside of a mouse for 24 h. As shown in Figure 5c, all tested areas showed the same results without the appearance of any erythema and edema, indicating that G−P−C@agarose gels were nontoxic and -irritating.

3.7. G−P−C@Agarose Gel Sensor Behaviors. The G−P−C@agarose gels exhibited good conductivity, self-adhesion, and biocompatibility, as well as the precise and stable response in electrical signals to deformation. To further investigate the sensing ability and potential applications in the healthcare of G−P−C@agarose gels, we designed and constructed a wearable biosensor with the gels. Figure 6a shows that the sensor was adhered to the knuckle of the index finger and recorded the four states during continuous finger bending. Furthermore, the small- and large-scale motion of wrist and arm bending could also be monitored (Figure 6b,c), and the signals were distinct and stable at least in five cycles. Besides those experiments, we pasted the sensor on the people's back to monitor sitting posture; the sensor resistance obviously increased when people hunched (Figure 6d), which may be applied to correct the wrong sitting posture. Therefore, it was reasonable to believe that G−P−C@agarose gels had a great potential application in the field of wearable devices.

4. CONCLUSIONS

In summary, biocompatible, conductive, and self-adhesive agarose gels are fabricated by the introduction of PDA−CNTs and glycerol. CNTs are modified by PDA to improve the

https://doi.org/10.1021/acsabm.1c00501
ACS Appl. Bio Mater. XXXX, XXX, XXX−XXX

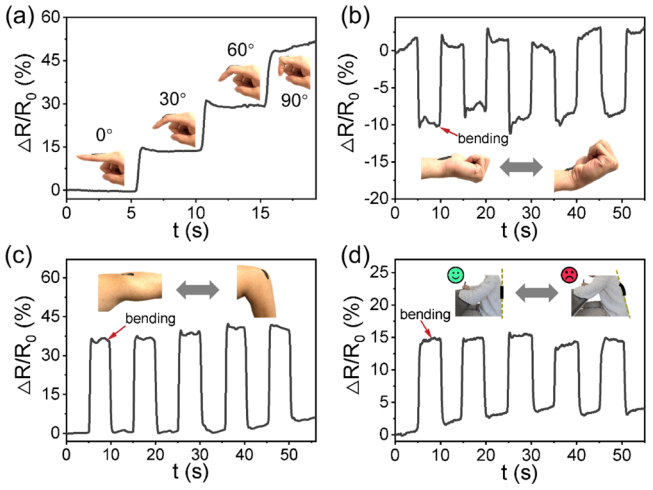

Figure 6. Body motions detected by the wearable biosensor based on G−P−C@agarose gels. (a) Finger, (b) inner wrist, (c) elbow joint, and (d) back bending. The insets show the gels directly adhered onto the finger, wrist, elbow, and back, respectively.

dispersity of CNTs in gel networks, which not only endows gels with excellent conductivity but also strongly enhances the mechanical properties such as tensile strength, stretchability, and self-healing capability. The further addition of glycerol makes the gels possess a good reversible adhesiveness to glass and metal substrates, especially to body tissues, while dramatically improving the stretchability of the gels. Meanwhile, heating/freezing tolerability and the moisture retention of the gels were enhanced significantly, which will keep the hydrogel intact after freezing (−20 °C) and heating (60 °C) treatment and maintain its initial state when exposed to an air atmosphere for 1 week at least. In addition, experimental data show that sensors based on G−P−C@agarose gels are able to detect the body motions precisely and quickly, which makes the gels suitable for future applications in wearable devices.

■ ASSOCIATED CONTENT

Supporting Information

The Supporting Information is available free of charge at https://pubs.acs.org/doi/10.1021/acsabm.1c00501.

Experimental details of preparation and characterization; EDS mapping and SEM graphs of raw CNTs and PDA−CNTs; photographs of PDA solutions; shear adhesion strength−displacement curves; photographs of gels with different glycerol contents; SEM graphs of the pure agarose gel and PDA−CNTs@agarose gel; AC impedance curves of pure water agarose hydrogels; conductive self-healing demonstration; 3ITT curves; and schematic illustration of the shear adhesion strength test, tensile and compress test, and conductivity test (PDF)

■ AUTHOR INFORMATION

Corresponding Authors

Anhe Wang − *State Key Laboratory of Biochemical Engineering, Institute of Process Engineering, Chinese Academy of Sciences, 100190 Beijing, China; University of Chinese Academy of Sciences, 100049 Beijing, China*; Email: ahwang@ipe.ac.cn

Jian Yin − *Key Laboratory of Carbohydrate Chemistry and Biotechnology, Ministry of Education, School of Biotechnology, Jiangnan University, 214122 Wuxi, China*; orcid.org/0000-0002-2284-1666; Email: jianyin@jiangnan.edu.cn

Shuo Bai − *State Key Laboratory of Biochemical Engineering, Institute of Process Engineering, Chinese Academy of Sciences, 100190 Beijing, China; University of Chinese Academy of Sciences, 100049 Beijing, China*; orcid.org/0000-0001-5360-3399; Email: baishuo@ipe.ac.cn

Authors

Qingquan Han − *State Key Laboratory of Biochemical Engineering, Institute of Process Engineering, Chinese Academy of Sciences, 100190 Beijing, China; University of Chinese Academy of Sciences, 100049 Beijing, China*

Wei Song − *Department of Electronic Engineering, Tsinghua University, 100084 Beijing, China*

Milin Zhang − *Department of Electronic Engineering, Tsinghua University, 100084 Beijing, China*

Shengtao Wang − *State Key Laboratory of Biochemical Engineering, Institute of Process Engineering, Chinese Academy of Sciences, 100190 Beijing, China; Key Laboratory of Carbohydrate Chemistry and Biotechnology, Ministry of Education, School of Biotechnology, Jiangnan University, 214122 Wuxi, China*

Peng Ren − *State Key Laboratory of Biochemical Engineering, Institute of Process Engineering, Chinese Academy of Sciences, 100190 Beijing, China; University of Chinese Academy of Sciences, 100049 Beijing, China*

Linna Hao − *State Key Laboratory of Biochemical Engineering, Institute of Process Engineering, Chinese Academy of Sciences, 100190 Beijing, China; Key Laboratory of Carbohydrate Chemistry and Biotechnology, Ministry of Education, School of Biotechnology, Jiangnan University, 214122 Wuxi, China*

Complete contact information is available at: https://pubs.acs.org/10.1021/acsabm.1c00501

Author Contributions

S.B., A.W., J.Y., and Q.H. designed the study. Q.H., W.S., and M.Z. performed the experiments and wrote the manuscript. S.W., P.R., and L.H. analyzed the data. All authors reviewed the manuscript.

Funding

Beijing Municipal Natural Science Foundation (7212206).

Notes

The authors declare no competing financial interest.

■ ACKNOWLEDGMENTS

We thank the mice used in this study.

■ ABBREVIATIONS

DA, dopamine; PDA, polydopamine; CNT(s), carbon nanotube(s); G−P−C, glycerol−polydopamine−carbon nanotubes; TEM, transmission electron microscopy; SEM, scanning electron microscopy; FTIR, Fourier-transform infrared spectrometry; UV−vis, ultraviolet−visible; CLSM, confocal laser scanning microscopy

https://doi.org/10.1021/acsabm.1c00501
ACS Appl. Bio Mater. XXXX, XXX, XXX−XXX

REFERENCES

(1) (a) Liu, X.; Zhang, M.; Richardson, A. G.; Lucas, T. H.; Van der Spiegel, J. Design of a Closed-Loop, Bidirectional Brain Machine Interface System With Energy Efficient Neural Feature Extraction and PID Control. *IEEE Trans. Biomed. Circuits Syst.* **2017**, *11*, 729−742. (b) Webb, R. C.; Bonifas, A. P.; Behnaz, A.; Zhang, Y.; Yu, K. J.; Cheng, H.; Shi, M.; Bian, Z.; Liu, Z.; Kim, Y.-S.; Yeo, W.-H.; Park, J. S.; Song, J.; Li, Y.; Huang, Y.; Gorbach, A. M.; Rogers, J. A. Ultrathin conformal devices for precise and continuous thermal characterization of human skin. *Nat. Mater.* **2013**, *12*, 938−944.

(2) Pantelopoulos, A.; Bourbakis, N. G. A survey on wearable sensor-based systems for health monitoring and prognosis. *IEEE Trans. Syst. Man Cybern. C Appl. Rev.* **2010**, *40*, 1−12.

(3) Liu, X.; Zhang, M.; Richardson, A. G.; Lucas, T. H.; Van der Spiegel, J. Design of a closed-loop, bidirectional brain machine interface system with energy efficient neural feature extraction and pid control. *IEEE Trans Biomed Circuits Syst.* **2017**, *11*, 729−742.

(4) Luo, D.; Zhang, M.; Wang, Z. A low-noise chopper amplifier designed for multi-channel neural signal acquisition. *IEEE J Solid-St. Circ.* **2019**, *54*, 2255−2265.

(5) Liu, X.; Sacks, J.; Zhang, M.; Richardson, A. G.; Lucas, T. H.; Van der Spiegel, J. The virtual trackpad: an electromyography-based, wireless, real-time, low-power, embedded hand-gesture-recognition system using an event-driven artificial neural network. *IEEE Trans. Circuits Syst. II* **2017**, *64*, 1257−1261.

(6) Tao, X.; Yi, W.; He, Y.; Lyu, S.; Xu, X. Q.; Liao, S.; Wang, Y. An intrinsically conductive elastomer for thromboembolism diagnosis. *Adv. Mater. Technol.* **2021**, *6*, 2001076.

(7) Gui, Q.; He, Y.; Gao, N.; Tao, X.; Wang, Y. A skin-inspired integrated sensor for synchronous monitoring of multiparameter signals. *Adv. Funct. Mater.* **2017**, *27*, 1702050.

(8) Gao, W.; Emaminejad, S.; Nyein, H. Y. Y.; Challa, S.; Chen, K.; Peck, A.; Fahad, H. M.; Ota, H.; Shiraki, H.; Kiriya, D.; Lien, D.-H.; Brooks, G. A.; Davis, R. W.; Javey, A. Fully integrated wearable sensor arrays for multiplexed in situ perspiration analysis. *Nature* **2016**, *529*, 509−514.

(9) Chan, M.; Estève, D.; Escriba, C.; Campo, E. A review of smart homes-present state and future challenges. *Comput. Methods Progr. Biomed.* **2008**, *91*, 55−81.

(10) Stoppa, M.; Chiolerio, A. Wearable electronics and smart textiles: a critical review. *Sensors* **2014**, *14*, 11957−11992.

(11) Kim, S. J.; We, J. H.; Cho, B. J. A wearable thermoelectric generator fabricated on a glass fabric. *Energy Environ. Sci.* **2014**, *7*, 1959−1965.

(12) Liu, X.; Yuk, H.; Lin, S.; Parada, G. A.; Tang, T. C.; Tham, E.; de la Fuente-Nunez, C.; Lu, T. K.; Zhao, X. 3D printing of living responsive materials and devices. *Adv. Mater.* **2018**, *30*, 1704821.

(13) Yuk, H.; Lu, B.; Zhao, X. Hydrogel bioelectronics. *Chem. Soc. Rev.* **2019**, *48*, 1642−1667.

(14) Liu, X.; Tang, T.-C.; Tham, E.; Yuk, H.; Lin, S.; Lu, T. K.; Zhao, X. Stretchable living materials and devices with hydrogel-elastomer hybrids hosting programmed cells. *Proc. Natl. Acad. Sci. U.S.A.* **2017**, *114*, 2200−2205.

(15) Song, W.; Wang, A.; Chen, Y.; Bai, S.; Han, Q.; Lin, Z.; Yan, N.; Luo, D.; Liao, Y.; Zhang, M.; Wang, Z.; Xie, X. Design of a flexible wearable smart semg recorder integrated gradient boosting decision tree based hand gesture recognition. *IEEE Trans Biomed Circuits Syst.* **2019**, *13*, 1563−1574.

(16) Shao, C.; Wang, M.; Meng, L.; Chang, H.; Wang, B.; Xu, F.; Yang, J.; Wan, P. Mussel-inspired cellulose nanocomposite tough hydrogels with synergistic self-healing, Adhesive, and Strain-Sensitive Properties. *Chem. Mater.* **2018**, *30*, 3110−3121.

(17) Tang, L.; Cheng, S.; Zhang, L.; Mi, H.; Mou, L.; Yang, S.; Huang, Z.; Shi, X.; Jiang, X. Printable metal-polymer conductors for highly stretchable bio-devices. *iScience* **2018**, *4*, 302−311.

(18) Ge, J.; Sun, L.; Zhang, F.-R.; Zhang, Y.; Shi, L.-A.; Zhao, H.-Y.; Zhu, H.-W.; Jiang, H.-L.; Yu, S.-H. A stretchable electronic fabric artificial skin with pressure-, lateral strain-, and flexion-sensitive properties. *Adv. Mater.* **2016**, *28*, 722−728.

(19) Lin, S.; Yuk, H.; Zhang, T.; Parada, G. A.; Koo, H.; Yu, C.; Zhao, X. Stretchable hydrogel electronics and devices. *Adv. Mater.* **2016**, *28*, 4497−4505.

(20) Deligkaris, K.; Tadele, T. S.; Olthuis, W.; van den Berg, A. Hydrogel-based devices for biomedical applications. *Sens. Actuators, B* **2010**, *147*, 765−774.

(21) Mogosanu, G. D.; Grumezescu, A. M. Natural and synthetic polymers for wounds and burns dressing. *Int. J. Pharm.* **2014**, *463*, 127−136.

(22) Li, J.; Xing, R.; Bai, S.; Yan, X. Recent advances of self-assembling peptide-based hydrogels for biomedical applications. *Soft Matter* **2019**, *15*, 1704−1715.

(23) Cui, C.; Fu, Q.; Meng, L.; Hao, S.; Dai, R.; Yang, J. Recent progress in natural biopolymers conductive hydrogels for flexible wearable sensors and energy devices: materials, structures, and performance. *ACS Appl. Bio Mater.* **2021**, *4*, 85−121.

(24) Chen, Q.; Zhu, L.; Zhao, C.; Wang, Q.; Zheng, J. A robust, one-pot synthesis of highly mechanical and recoverable double network hydrogels using thermoreversible sol-gel polysaccharide. *Adv. Mater.* **2013**, *25*, 4171−4176.

(25) Han, Q.; Chen, Y.; Song, W.; Zhang, M.; Wang, S.; Ren, P.; Hao, L.; Wang, A.; Bai, S.; Yin, J. Fabrication of agarose hydrogel with patterned silver nanowires for motion sensor. *Bio-Des. Manuf.* **2019**, *2*, 269−277.

(26) Hur, J.; Im, K.; Kim, S. W.; Kim, J.; Chung, D.-Y.; Kim, T.-H.; Jo, K. H.; Hahn, J. H.; Bao, Z.; Hwang, S.; Park, N. Polypyrrole/agarose-based electronically conductive and reversibly restorable hydrogel. *ACS Nano* **2014**, *8*, 10066−10076.

(27) Hu, Y.; Du, Z.; Deng, X.; Wang, T.; Yang, Z.; Zhou, W.; Wang, C. Dual physically cross-linked hydrogels with high stretchability, toughness, and good self-recoverability. *Macromolecules* **2016**, *49*, 5660−5668.

(28) Rauner, N.; Meuris, M.; Zoric, M.; Tiller, J. C. Enzymatic mineralization generates ultrastiff and tough hydrogels with tunable mechanics. *Nature* **2017**, *543*, 407−410.

(29) Gaharwar, A. K.; Dammu, S. A.; Canter, J. M.; Wu, C.-J.; Schmidt, G. Highly extensible, tough, and elastomeric nanocomposite hydrogels from poly(ethylene glycol) and hydroxyapatite nanoparticles. *Biomacromolecules* **2011**, *12*, 1641−1650.

(30) Son, D.; Kang, J.; Vardoulis, O.; Kim, Y.; Matsuhisa, N.; Oh, J. Y.; To, J. W.; Mun, J.; Katsumata, T.; Liu, Y.; McGuire, A. F.; Krason, M.; Molina-Lopez, F.; Ham, J.; Kraft, U.; Lee, Y.; Yun, Y.; Tok, J. B.-H.; Bao, Z. An integrated self-healable electronic skin system fabricated via dynamic reconstruction of a nanostructured conducting network. *Nat. Nanotechnol.* **2018**, *13*, 1057−1065.

(31) Liu, X.; Lu, C.; Wu, X.; Zhang, X. Self-healing strain sensors based on nanostructured supramolecular conductive elastomers. *J. Mater. Chem. A* **2017**, *5*, 9824−9832.

(32) Yuan, T.; Cui, X.; Liu, X.; Qu, X.; Sun, J. Highly tough, stretchable, self-healing, and recyclable hydrogels reinforced by in situ-formed polyelectrolyte complex nanoparticles. *Macromolecules* **2019**, *52*, 3141−3149.

(33) Lee, H.; Dellatore, S. M.; Miller, W. M.; Messersmith, P. B. Mussel-inspired surface chemistry for multifunctional coatings. *Science* **2007**, *318*, 426−430.

(34) Chao, C.; Liu, J.; Wang, J.; Zhang, Y.; Zhang, B.; Zhang, Y.; Xiang, X.; Chen, R. Surface modification of halloysite nanotubes with dopamine for enzyme immobilization. *ACS Appl. Mater. Interfaces* **2013**, *5*, 10559−10564.

(35) Xing, J.; Wang, Q.; He, T.; Zhou, Z.; Chen, D.; Yi, X.; Wang, Z.; Wang, R.; Tan, G.; Yu, P.; Ning, C. Polydopamine-assisted immobilization of copper ions onto hemodialysis membranes for antimicrobial. *ACS Appl. Bio Mater.* **2018**, *1*, 1236−1243.

(36) Cui, C.; Wu, T.; Gao, F.; Fan, C.; Xu, Z.; Wang, H.; Liu, B.; Liu, W. An autolytic high strength instant adhesive hydrogel for emergency self-rescue. *Adv. Funct. Mater.* **2018**, *28*, 1804925.

(37) Liu, X.; Zhang, Q.; Gao, Z.; Hou, R.; Gao, G. Bioinspired adhesive hydrogel driven by adenine and thymine. *ACS Appl. Mater. Interfaces* **2017**, *9*, 17645−17652.

https://doi.org/10.1021/acsabm.1c00501
ACS Appl. Bio Mater. XXXX, XXX, XXX−XXX

(38) Yuk, H.; Varela, C. E.; Nabzdyk, C. S.; Mao, X.; Padera, R. F.; Roche, E. T.; Zhao, X. Dry double-sided tape for adhesion of wet tissues and devices. *Nature* **2019**, *575*, 169−174.
(39) Brubaker, C. E.; Messersmith, P. B. Enzymatically degradable mussel-inspired adhesive hydrogel. *Biomacromolecules* **2011**, *12*, 4326−4334.
(40) Liang, S.; Zhang, Y.; Wang, H.; Xu, Z.; Chen, J.; Bao, R.; Tan, B.; Cui, Y.; Fan, G.; Wang, W.; Wang, W.; Liu, W. Paintable and rapidly bondable conductive hydrogels as therapeutic cardiac patches. *Adv. Mater.* **2018**, *30*, 1704235.
(41) Rao, P.; Sun, T. L.; Chen, L.; Takahashi, R.; Shinohara, G.; Guo, H.; King, D. R.; Kurokawa, T.; Gong, J. P. Tough hydrogels with fast, strong, and reversible underwater adhesion based on a multiscale design. *Adv. Mater.* **2018**, *30*, 1801884.
(42) Mahdavi, A.; Ferreira, L.; Sundback, C.; Nichol, J. W.; Chan, E. P.; Carter, D. J. D.; Bettinger, C. J.; Patanavanich, S.; Chignozha, L.; Ben-Joseph, E.; Galakatos, A.; Pryor, H.; Pomerantseva, I.; Masiakos, P. T.; Faquin, W.; Zumbuehl, A.; Hong, S.; Borenstein, J.; Vacanti, J.; Langer, R.; Karp, J. M. A biodegradable and biocompatible gecko-inspired tissue adhesive. *Proc. Natl. Acad. Sci. U.S.A.* **2008**, *105*, 2307−2312.
(43) Sartori, T.; Feltre, G.; do Amaral Sobral, P. J.; da Cunha, R. L.; Menegalli, F. C. Biodegradable pressure sensitive adhesives produced from vital wheat gluten: Effect of glycerol as plasticizer. *Colloids Surf., A* **2019**, *560*, 42−49.
(44) Ren, Y.; Barringer, S. A. Adhesion of sugar and oil solutions. *J. Food Process. Preserv.* **2009**, *33*, 427−435.
(45) Liu, Y.; Ai, K.; Lu, L. Polydopamine and its derivative materials: synthesis and promising applications in energy, environmental, and biomedical fields. *Chem. Rev.* **2014**, *114*, 5057−5115.
(46) Ding, Y.; Weng, L.-T.; Yang, M.; Yang, Z.; Lu, X.; Huang, N.; Leng, Y. Insights into the aggregation/deposition and structure of a polydopamine film. *Langmuir* **2014**, *30*, 12258−12269.
(47) Zhang, C.; Lv, Y.; Qiu, W.-Z.; He, A.; Xu, Z.-K. Polydopamine coatings with nanopores for versatile molecular separation. *ACS Appl. Mater. Interfaces* **2017**, *9*, 14437−14444.
(48) Lin, Y.-S.; Abadeer, N.; Hurley, K. R.; Haynes, C. L. Ultrastable, redispersible, small, and highly organomodified mesoporous silica nanotherapeutics. *J. Am. Chem. Soc.* **2011**, *133*, 20444−20457.
(49) Ci, Q.; Liu, J.; Qin, X.; Han, L.; Li, H.; Yu, H.; Lim, K.-L.; Zhang, C.-W.; Li, L.; Huang, W. Polydopamine dots-based fluorescent nanoswitch assay for reversible recognition of glutamic acid and Al^{3+} in human serum and living cell. *ACS Appl. Mater. Interfaces* **2018**, *10*, 35760−35769.
(50) Zhao, Z.; Guo, L.; Feng, L.; Lu, H.; Xu, Y.; Wang, J.; Xiang, B.; Zou, X. Polydopamine functionalized graphene oxide nanocomposites reinforced the corrosion protection and adhesion properties of waterborne polyurethane coatings. *Eur. Polym. J.* **2019**, *120*, 109249.
(51) Du, X.; Li, L.; Li, J.; Yang, C.; Frenkel, N.; Welle, A.; Heissler, S.; Nefedov, A.; Grunze, M.; Levkin, P. A. UV-triggered dopamine polymerization: control of polymerization, surface coating, and photopatterning. *Adv. Mater.* **2014**, *26*, 8029−8033.
(52) Yu, F.; Chen, S.; Chen, Y.; Li, H.; Yang, L.; Chen, Y.; Yin, Y. Experimental and theoretical analysis of polymerization reaction process on the polydopamine membranes and its corrosion protection properties for 304 Stainless Steel. *J. Mol. Struct.* **2010**, *982*, 152−161.
(53) Yu, X.; Fan, H.; Wang, L.; Jin, Z. Formation of polydopamine nanofibers with the aid of folic acid. *Angew. Chem., Int. Ed.* **2014**, *53*, 12600−12604.
(54) Centeno, S. A.; Shamir, J. Surface enhanced Raman scattering (SERS) and FTIR characterization of the sepia melanin pigment used in works of art. *J. Mol. Struct.* **2008**, *873*, 149−159.
(55) Han, L.; Liu, K.; Wang, M.; Wang, K.; Fang, L.; Chen, H.; Zhou, J.; Lu, X. Mussel-inspired adhesive and conductive hydrogel with long-lasting moisture and extreme temperature tolerance. *Adv. Funct. Mater.* **2018**, *28*, 1704195.
(56) Chen, F.; Zhou, D.; Wang, J.; Li, T.; Zhou, X.; Gan, T.; Handschuh-Wang, S.; Zhou, X. Rational fabrication of anti-freezing, non-drying tough organohydrogels by one-pot solvent displacement. *Angew. Chem., Int. Ed.* **2018**, *57*, 6568−6571.
(57) Liao, M.; Wan, P.; Wen, J.; Gong, M.; Wu, X.; Wang, Y.; Shi, R.; Zhang, L. Wearable, healable, and adhesive epidermal sensors assembled from mussel-inspired conductive hybrid hydrogel framework. *Adv. Funct. Mater.* **2017**, *27*, 1703852.
(58) Lu, N.; Na, R.; Li, L.; Zhang, C.; Chen, Z.; Zhang, S.; Luan, J.; Wang, G. Rational design of antifreezing organohydrogel electrolytes for flexible supercapacitors. *ACS Appl. Energy Mater.* **2020**, *3*, 1944−1951.
(59) Cai, G.; Wang, J.; Qian, K.; Chen, J.; Li, S.; Lee, P. S. Extremely stretchable strain sensors based on conductive self-healing dynamic cross-links hydrogels for human-motion detection. *Adv. Sci.* **2017**, *4*, 1600190.
(60) Guo, M.; Wu, Y.; Xue, S.; Xia, Y.; Yang, X.; Dzenis, Y.; Li, Z.; Lei, W.; Smith, A. T.; Sun, L. A highly stretchable, ultra-tough, remarkably tolerant, and robust self-healing glycerol-hydrogel for a dual-responsive soft actuator. *J. Mater. Chem. A* **2019**, *7*, 25969−25977.
(61) Chen, T.; Hao, R.; Peng, H.; Dai, L. High-performance, stretchable, wire-shaped supercapacitors. *Angew. Chem., Int. Ed.* **2015**, *54*, 618−622.
(62) Wu, J.; Wu, Z.; Xu, H.; Wu, Q.; Liu, C.; Yang, B.-R.; Gui, X.; Xie, X.; Tao, K.; Shen, Y.; Miao, J.; Norford, L. K. An intrinsically stretchable humidity sensor based on anti-drying, self-healing and transparent organohydrogels. *Mater. Horiz.* **2019**, *6*, 595−603.
(63) Chen, Z.; To, J. W. F.; Wang, C.; Lu, Z.; Liu, N.; Chortos, A.; Pan, L.; Wei, F.; Cui, Y.; Bao, Z. A three-dimensionally interconnected carbon nanotube-conducting polymer hydrogel network for high-performance flexible battery electrodes. *Adv. Energy Mater.* **2014**, *4*, 1400207.
(64) Ren, P.; Li, J.; Zhao, L.; Wang, A.; Wang, M.; Li, J.; Jian, H.; Li, X.; Yan, X.; Bai, S. Dipeptide self-assembled hydrogels with shear-thinning and instantaneous self-healing properties determined by peptide sequences. *ACS Appl. Mater. Interfaces* **2020**, *12*, 21433−21440.
(65) Jian, H.; Wang, M.; Dong, Q.; Li, J.; Wang, A.; Li, X.; Ren, P.; Bai, S. Dipeptide self-assembled hydrogels with tunable mechanical properties and degradability for 3D bioprinting. *ACS Appl. Mater. Interfaces* **2019**, *11*, 46419−46426.
(66) Zheng, Y.; Ouyang, W.-Q.; Wei, Y.-P.; Syed, S.; Hao, C.-S.; Wang, B.-Z.; Shang, Y.-H. Effects of Carbopol 934 proportion on nanoemulsion gel for topical and transdermal drug delivery: a skin permeation study. *Int. J. Nanomed.* **2016**, *11*, 5971−5987.

https://doi.org/10.1021/acsabm.1c00501
ACS Appl. Bio Mater. XXXX, XXX, XXX−XXX